ELSEVIER

Contents lists available at ScienceDirect

## International Journal of Greenhouse Gas Control

journal homepage: www.elsevier.com/locate/ijggc



# Analytical first-principles-based model for sprays-based CO<sub>2</sub> capture

Awan Bhati, Serhat Bilyaz, Vaibhay Bahadur

Walker Department of Mechanical Engineering, The University of Texas at Austin, Austin, TX

#### ARTICLE INFO

Keywords:
Carbon capture
mass transfer
capture efficiency
solvent loading
flue gas
effective surface area

#### ABSTRACT

 $CO_2$  removal from flue gases or air is directly proportional to the overall contact area between the solvent and gas flow. Spraying the solvent offers possibilities for large area/volume ratios resulting from the small size of solvent droplets. The overall mass transfer  $(K_GA_\nu)$  is a crucial indicator of the performance of the system and indicates the overall  $CO_2$  capture rate per unit volume at given working pressure. The maximum capture rate of spray systems considered in this study is  $608 \text{ kmol/m}^3$ -hr. This study develops an analytical model to predict mass transfer in spray-based systems for  $CO_2$  capture by evaluating  $K_GA_\nu$  and capture efficiency. Model predictions are validated using two experimental studies for a range of liquid flow rate, inlet solvent loading, different nozzle types, and inlet  $CO_2$  partial pressure. The relative importance of the incorporation of equilibrium partial pressure of  $CO_2$   $(P^*)$  into amine with respect to  $CO_2$  partial pressure is also studied. It is found that its effect on  $K_GA_\nu$  is prominent in high liquid flow rate and low solvent loading regimes where the overall  $CO_2$  capture is high. Finally, the variation of key parameters such as  $K_GA_\nu$ , total mass transfer coefficient  $(K_G)$ , effective area  $(A_\nu)$ , solvent loading (a), and mole fraction of  $CO_2$  in the gas stream  $(K_{CO_2})$  along the channel height is studied, which gives insights on optimization of the channel height for specified operating conditions.

#### 1. Introduction

The Paris agreement aims for net-zero  $\mathrm{CO}_2$  emission by the year 2050 to address anthropogenic climate change (Garg et al., 2017). Carbon capture and sequestration (CCS) will be vital to achieving net-zero targets. The current operational CCS capacity is around 40Mt per annum, while the net greenhouse gas emissions in 2021 is estimated at 52.8 Gt  $\mathrm{CO}_2$  (Garg et al., 2017). While the economic viability of CCS is highest at power plants where  $\mathrm{CO}_2$  is emitted (point-source capture), it is increasingly likely that  $\mathrm{CO}_2$  would need to be captured directly from air, also called as Direct Air Capture (DAC) (Stolaroff et al., 2008).

A typical CO<sub>2</sub> capture system, whether it be point-source capture or direct air capture, consists of an absorber and a stripper (Stolaroff et al., 2008, Yates et al., 2017). The absorber captures CO<sub>2</sub> using solid sorbents or liquid solvents and convert it into salts. Monoethanolamine (MEA), methyldiethanolamine (MDEA), diethanolamine (DEA), sodium-hydroxide (NaOH), Calcium oxide (CaO), etc. are some of the solvents used for CO<sub>2</sub> capture (Chen et al., 2005, Niu et al., 2009, Tamhankar et al., 2015, Kuntz and Aroonwilas, 2008, Kuntz and Aroonwilas, 2009). Gas absorption from an aqueous alkanolamine solution is the most well-established method for CO<sub>2</sub> capture (Davison et al.). The CO<sub>2</sub> loaded solvents are passed into the stripper where they

are heated to remove CO2, which allows reuse of the solvent. Absorbers are designed to attain maximum CO2 capture by enhancing gas-liquid contact area and thus mass transfer between the liquid solvent and CO2 rich gas stream. This is typically achieved by packed beds or spray-based systems (Kuntz and Aroonwilas, 2008, Yeh and Rochelle, 2003, Demontigny et al., 2005). A packed bed enables solvent redistribution into thin films when the solvent hits the packing bead material, which increases the contact area. The packing arrangement can be randomly arranged, structured, or be a hybrid. Packing material can be metal, ceramic, or plastic. Three primary attributes that determine mass transfer have been studied for random and structured packing (Wang et al., 2012): effective area  $(a_e)$ , gas mass transfer coefficient  $(k_\sigma)$ , and liquid mass transfer coefficient ( $k_I$ ). The effective area was found to increase with liquid flow rate until it asymptotes at the packing material surface area which varies from 100-300 m<sup>2</sup>/m<sup>3</sup>. Gas and liquid side mass transfer coefficients are strong functions of gas and liquid velocities respectively. Several models have been developed to obtain these three parameters for a packed bed, some of which are reviewed in Flagiello et al. (2021).

A typical spray-based capture system consists of a nozzle at the top of the reactor which atomizes liquid solvent into small droplets typically of size 50-250  $\mu m.$  This increases effective contact area between the liquid and gas streams, which can be co-current or counter-current. A spray

E-mail address: vb@austin.utexas.edu (V. Bahadur).

<sup>\*</sup> Corresponding author.

Nomenclature			Equilibrium CO <sub>2</sub> partial pressure at given CO <sub>2</sub> loading and temperature			
$A_d$	Area of single droplet (m <sup>2</sup> )	$P_{tot}$	Total operating pressure (kPa)			
$A_{\nu}$	Effective mass transfer cross-sectional area (m <sup>2</sup> /m <sup>3</sup> )	$\dot{O}_G$	Gas flow rate (m <sup>3</sup> /s)			
$C^i_{CO_2}$	Concentration of CO <sub>2</sub> at inlet	$\dot{Q}_G \ Q_G^{"}$	Flux of gas flow rate (m <sup>3</sup> /m <sup>2</sup> -h)			
Cinit	Initial concentration of MEA (kmol/m <sup>3</sup> )		Liquid flow rate (m <sup>3</sup> /s)			
d	Droplet diameter (µm)	$\overset{.}{Q_L}_{{U}}$	Flux of liquid flow rate $(m^3/m^2-h)$			
D	Diameter of the channel (m)	R	Universal gas constant (= 8.314 kJ/kmol-K)			
$D_{CO_2,g}$	Diffusivity of CO <sub>2</sub> in gas phase (m <sup>2</sup> /s)	T	Temperature (K)			
$D_{CO_2,MEA}$	Diffusivity of CO <sub>2</sub> in liquid phase (m <sup>2</sup> /s)	U	Relative velocity of single droplet with respect to gas			
$G_I$	Inert gas flow rate (m <sup>3</sup> /m <sup>2</sup> -h)		stream (m/s)			
$H_{CO_2,MEA}$	Henry's constant for solubility of CO <sub>2</sub> in amine (kPa-m <sup>3</sup> /	$U_{\mathrm{G}}$	Absolute velocity of gas stream (m/s)			
	kmol)	$V_d$	Volume of single droplet (m <sup>3</sup> )			
Н	Height of the channel (m)	$v_d$	Absolute velocity of single droplet (m/s)			
J	Flux of CO <sub>2</sub> absorption (kmol/m <sup>2</sup> -h)	$X_{CO_2}$	Mole fraction of CO <sub>2</sub> in gas stream			
$K_G$	Total mass transfer coefficient (kmol/m²-h-kPa)	$X_{CO_2,in}$	Mole fraction of CO <sub>2</sub> in gas stream at inlet			
$k_g$	Mass transfer coefficient of gas phase (kmol/m²-h-kPa)	$X_{CO_2,out}$	Mole fraction of CO <sub>2</sub> in gas stream at exit			
$k_L$	Reactive mass transfer coefficient of liquid phase (kmol/	$Y_{CO_2}$	Mole ratio of CO <sub>2</sub> to N <sub>2</sub> in gas stream			
	m <sup>2</sup> -h-kPa)	Z	Distance along channel (m)			
$k_2$	Second-order reaction rate constant (m³/mol-s)	0 1 01				
$n_{CO_2}$	Mole flow rate of CO <sub>2</sub> consumed (mol/s)	Greek Ch				
$n_{MEA.free}$	Moles of free amine in solvent	α	Solvent loading (mole CO <sub>2</sub> / mole solvent)			
$n_{CO_2,cons}$	Moles of CO <sub>2</sub> consumed	$\alpha_{in}$	Solvent loading at liquid inlet			
$n_{tot}$	Total mole flow rate of gas (mol/s)	$\rho_w$	Density of water $(kg/m^3)$			
N	Number of droplets per unit length (m <sup>-1</sup> )	$\rho_{g}$	Density of gas (kg/m³)  Vinematic viscosity of gas (m²/s)			
$\dot{N}$	Rate of droplet generation (1/s)	$v_g$	Kinematic viscosity of gas (m <sup>2</sup> /s) Capture efficiency (%)			
$n_d$	Number of droplets	η	Capture enriciency (%)			
$P_{CO_2}$	Partial pressure of CO <sub>2</sub> in gas phase (kPa)					

Table 1
Summary of studies on spray-based CO<sub>2</sub> capture.

Reference	$\begin{array}{c} \text{Inlet CO}_2 \\ \text{Composition} \end{array}$	Solvent Used	Key Finding
(Kuntz and Aroonwilas, 2008, Kuntz and Aroonwilas, 2009)	5-15 vol%	MEA	Performance of spray is 2-7 times higher than that of packing
(Javed et al., 2010)	2.5 vol%	NaOH	Swirling inlet gas flow increases $K_G A_v$ by 31-49%
(Tamhankar et al., 2015)	12 mol%	NaOH	$K_GA_\nu$ was obtained at two different heights within the channel
(Ma et al., 2013)	10-20 kPa	$NH_3$	Highest $K_G A_{\nu}$ is for 15kPa and gas temperature 30-40 °C
(Zimmermann et al., 2017)	15 vol%	MEA	Variation along column height was studied
(Wu et al., 2018)	8-18 vol%	MEA	Diameter varying reactor used for experiments and simulations
(Xu et al., 2021)	15 vol%	NH <sub>3</sub> + PZ	Upward and downward liquid injection was compared
(Stolaroff et al., 2008)	Air	NaOH	Cost of CO <sub>2</sub> capture ranges between 53-127 \$/ton-CO <sub>2</sub> .

system removes the need of extra material that a packing bed would require. Furthermore, a spray system enables better visualization of the absorber as compared to a packed bed. Despite these advantages, there are very limited studies on  $\rm CO_2$  capture using spray-based systems (Yeh and Rochelle, 2003). Key studies are outlined in Table 1.

An experimental study was conducted using MEA to compare packed

beds and sprays by evaluating the performance parameter  $K_GA_{\nu}$  for each system (Kuntz and Aroonwilas, 2008, Kuntz and Aroonwilas, 2009). This parameter is the overall mass transfer coefficient and describes the overall CO2 capture rate per unit volume at given working pressure. A spray-based reactor using three different nozzles was compared with Mellapak 500Y packing. It was found that the system's performance was heavily dependent on solvent flow rate and the spray system provided a 2-7 times higher  $K_GA_V$  than packing. The Sauter Mean Diameter (SMD) in a spray system describes the maximum possible contact area between the solvent and gas for given solvent flow rate. It was found to vary roughly by 30% along radial distance within the channel (Tamhankar et al., 2014). Parameters such as  $K_GA_V$ , SMD and planar surface area were experimentally evaluated at two different heights within the channel and along radial distance, for different flow rates and inlet loading conditions (Tamhankar et al., 2015). It was found that inlet loading did not affect planar surface area significantly, however  $K_GA_V$ was heavily dependent on the inlet loading. An experimental study with ammonia as the solvent was conducted and  $K_GA_V$  was observed to increase with ammonia concentration, liquid to gas flow rate, and gas flow rate (Ma et al., 2013). The highest  $K_GA_V$  was found for inlet gas flow condition of 15 kPa CO<sub>2</sub> partial pressure and temperature of 30-40°C.

The traditional spray design was also modified in several different ways to obtain better system performance. The influence of a swirling inlet gas flow on  $K_GA_\nu$  has been studied and a 31-49% enhancement with respect to axial inlet gas flow was observed (Javed et al., 2010). Another experimental study using three spray columns connected in series was conducted to obtain the variation of solvent loading and  $CO_2$  concentration along channel height (Zimmermann et al., 2017). This also studied the influence of solvent loading and temperature on solvent properties and overall  $CO_2$  removal rate. A diameter varying reactor along with dual nozzle impinging MEA from two sides was studied experimentally and via ANSYS simulations (Wu et al., 2018). It was found that this system doubles the overall effective area when compared

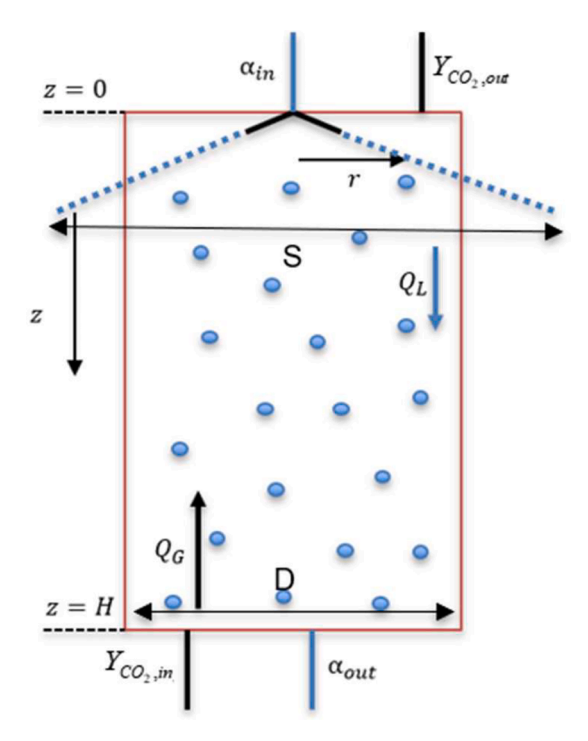


**Fig. 1.** Schematic showing modeling domain for typical spray-based CO<sub>2</sub> absorbers.

to traditional single nozzle spray tower. An air-blast atomizing column using MEA and NaOH as solvents was studied and MEA was found to result in better overall performance (Li et al., 2019). Thermophysical properties of solvent blends of ammonia and piperazine (PZ) were experimentally evaluated (Xu et al., 2021), and used in an ANSYS model to compare upward and downward liquid injection. It was found that upward injection increased droplet residence time, thus improving overall CO2 capture. A numerical study was conducted to study flow within a single droplet; a vortex was found within the droplet enhancing mixing between fresh solvent and solvent that has captured CO<sub>2</sub> (Chen et al., 2013). Furthermore, (Stolaroff et al., 2008) includes a technoeconomic analysis to ascertain the feasibility of using NaOH to capture CO2 from air using sprays; different channel heights and liquid flow rates were considered. The cost of CO2 capture in the absorber was found to range from 53-127 \$/ton-CO2. This excluded costs in the stripper for solvent recovery and CO<sub>2</sub> sequestration. Niu et al. (2009) found that the equivalence ratio of NaOH to CO2 is the key parameter affecting CO2 removal efficiency.

We highlight key research opportunities from the above literature survey, which motivate this study. Firstly, the solvents used in the limited studies in Table 1 are either MEA, NaOH or ammonia. More detailed studies are needed with additional solvents to get sufficient data for an in-depth understanding of the benefits of sprays. Secondly, while modeling can provide such understanding, the models developed to date have been validated to a very limited extent (primarily by the same group that does experiments). There is no universal model that has been validated across multiple studies, which could serve as the basis for the development of a new sprays-based CO<sub>2</sub> capture plant. Previous studies on modeling are either completely empirical in nature, or are ANSYS simulations which requires extensive computational resources.

This study develops a first-principles-based analytical model that is validated with experiments (Tamhankar et al., 2015, Kuntz and Aroonwilas, 2009) on spray-based  $\rm CO_2$  capture using aqueous MEA as the solvent. The model can be extended for use with any solvent or solvent blend as long as the relevant thermophysical properties of the solvent or solvent blend are known. The presently developed model has a computation time of < 3s for a specific working condition, and is much

faster than traditional computational fluid dynamics simulations. In addition to the fundamental nature of this model, it is also a convenient tool to study the detailed performance of the sprays-based absorber for specified operating conditions and sizes as it provides insights into the variation of key parameters such as  $K_GA_V$ , total mass transfer coefficient  $(K_G)$ , effective area  $(A_V)$ , solvent loading  $(\alpha)$ , and mole fraction of  $CO_2$  in the gas stream  $(X_{CO_2})$  along the channel height. This tool can thus enable optimization of the absorber design in addition to easily providing key inputs for techno-economic analysis.

#### 2. Mathematical Model

A typical spray-based  $CO_2$  absorber has a cylindrical geometry symmetric around r=0 and is schematically shown in Fig. 1. Lean solvent is introduced from the top (z=0) via a spray. The lean solvent can be fresh  $(\alpha_{in}=0)$  or  $CO_2$  loaded  $(\alpha_{in}>0)$ . After capturing  $CO_2$ , the rich solvent exits from the bottom of the channel (z=H).  $CO_2$  rich gas stream  $(Y_{CO_2,in})$  is introduced from the bottom and the  $CO_2$  lean gas stream exits from the top  $(Y_{CO_2,out})$ . The system is operated at a known inlet gas stream and solvent loading conditions, along with other operating parameters like liquid flow rate  $(\dot{Q}_L)$ , gas flow rate  $(\dot{Q}_G)$ , total pressure  $(P_{tot})$ , temperature (T), etc. Using these operating parameters, the variation of  $Y_{CO_2}$  and  $\alpha$  within the reactor can be evaluated by the given model. Eq. (1) can be used to estimate the flux of  $CO_2$  absorption (Javed et al., 2010).

$$J = K_G(P_{CO_2} - P^*) (1)$$

Here,  $P_{CO_2}$  is partial pressure of CO<sub>2</sub> in gas stream and  $P^*$  is equilibrium partial pressure of CO<sub>2</sub> for a given amine loading and temperature.  $P^*$  can be obtained using Eq. (2) (Xu and Rochelle, 2011).

$$P^* = \exp(39.3 - 12155 / T - 19\alpha^2 + 1105\alpha / T + 12800\alpha^2 / T)$$
 (2)

 $K_G$  is the overall mass transfer coefficient which is obtained according to the two-film theory from both gas-side and liquid-side mass transfer coefficients as described in Eq. (3) (Ramezani et al., 2021). The gas side mass transfer coefficient ( $k_g$ ) is obtained from Sherwood number correlation for a falling droplet in countercurrent flow. The reactive liquid side mass transfer coefficient ( $k_L$ ) incorporates both reaction kinetics and liquid side mass transfer boundary layer.

$$\frac{1}{K_G} = \frac{1}{k_e} + \frac{1}{k_L} \tag{3}$$

The two mass transfer coefficients can be obtained from the equations below (Ramezani et al., 2021), where  $C_{init}$  is the concentration of amine at the inlet,  $D_{CO_2,MEA}$  is the diffusivity of CO<sub>2</sub> in the amine solution,  $D_{CO_2,g}$  is the diffusivity of CO<sub>2</sub> in the gas stream, and  $H_{CO_2}$  is Henry's constant for solubility of CO<sub>2</sub> in amine solution.

$$k_g = \left(\frac{D_{CO_2,g}}{RTd}\right) \left(2 + 0.552 * \left(\frac{Ud}{\nu_g}\right)^{0.5} \left(\frac{\nu_g}{D_{CO_2,g}}\right)^{1/5}\right)$$
(4)

$$k_{L} = \frac{\sqrt{k_{2}C_{init}(1 - 2\alpha)D_{CO_{2},MEA}}}{H_{CO_{2}}}$$
 (5)

The chemical reactions involved in  $CO_2$  absorption are described in the equations below (Ramezani et al., 2021). The first reaction is the stage of zwitterion (RNH $_2^+$ COO $^-$ ) formation as an intermediate. In the second stage, RNH $_2^+$ COO $^-$  undergoes deprotonation by a base B to form carbamate (RNHCOO $^-$ ). In these reactions, B could be an amine,  $CO_3^{2-}$ ,  $HCO_3^{-}$ ,  $H_2O$  or  $OH^-$  (Ramachandran et al., 2006).

$$CO_2 + RNH_2 \leftrightarrow RNH_2^+COO^- \tag{6}$$

$$RNH_2^+COO^- + B \leftrightarrow RNHCOO^- + BH^+ \tag{7}$$

Upon considering the zwitterion formation step as the rate

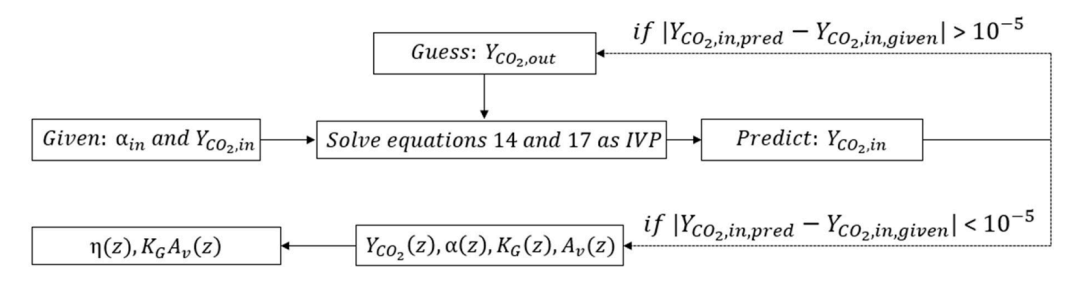


Fig. 2. Block diagram outlining the procedure for solving the system of equations in the model.

determining step, the reaction rate between MEA and  $CO_2$  can be described as per the equation below.  $k_2$  is the forward reaction constant for zwitterion formation reaction; its value can be obtained for aqueous MEA solutions from empirical relations (Versteeg et al., 1996).

$$R_{CO_2} = k_2 [MEA][CO_2] \tag{8}$$

Next, a parameter N is defined as the number of droplets per unit distance along channel height as shown in Eq. (9). This parameter captures droplet density and can be evaluated in terms of droplet size, velocity and liquid flow rate as described in Eq. (10) where the factor f estimates the fraction of liquid in the form of droplets. The factor f is considered to be equal to 1 when the spread associated with the spray (S) is smaller than the channel diameter (D), and is equal to D/S when D<S. The spread of the spray (S) is obtained from correlations provided in (Lim et al., 2013).

$$N = \frac{dn_d}{dz} \tag{9}$$

$$N = \frac{\dot{Q}_L}{v_L V_c} f \tag{10}$$

Using the droplet density, area of each droplet, and the flux of  $CO_2$  absorption, the rate of moles of  $CO_2$  captured per unit distance along channel can be obtained as shown in Eq. (11).

$$\frac{d\dot{n}_{CO_2}}{dz} = JNA_d \tag{11}$$

The rate of moles of  $CO_2$  captured can also be expressed using the mole flow rate of inert gas  $(N_2)$  and the change in mole ratio of  $CO_2$  to  $N_2$  as shown in Eq. (12). The mole flow rate of  $N_2$  can be obtained assuming ideal gas law as shown in Eq. (13).

$$d\dot{n}_{CO_2} = \dot{n}_{N_2} dY_{CO_2} \tag{12}$$

$$n_{N_2} = \frac{Q_{N_2} P_{tot}}{RT} \tag{13}$$

Substituting into Eq. (11), and rearranging, the variation of mole ratio of  $CO_2$  along column height can be expressed as shown in Eq. (14) below.

$$\frac{dY_{CO_2}}{dz} = K_G RT \frac{\dot{Q}_L}{\dot{Q}_{N_2}} \frac{A_d}{v_d V_d} \left( \frac{Y_{CO_2}}{1 + Y_{CO_2}} - \frac{P^*}{P_{tot}} \right)$$
 (14)

For the liquid side, the change in loading of solvent is described by Eq. (15). The rate of absorption of  $CO_2$  into liquid is the same as the rate at which  $CO_2$  is removed from the gas phase as shown in Eq. (16).

$$\alpha = \frac{n_{CO_2,init} + n_{CO_2,cons}}{n_{MEA,init}} = \alpha_{in} + \frac{n_{CO_2,cons}}{n_{MEA,init}}$$
(15)

$$\frac{d\dot{n}_{CO_2}|_{in,liq}}{dz} = \frac{d\dot{n}_{CO_2}|_{out,gas}}{dz}$$
(16)

The rate of moles of  $CO_2$  consumed in the liquid phase can also be expressed as  $dn_{CO_2}|_{liq} = Q_L C_{init} d\alpha$ . Upon applying this relation with Eq.s (12)–(16), and rearranging, the variation of amine loading with distance

can be obtained as described in Eq. (17) below.

$$\frac{d\alpha}{dz} = \frac{P_{tot}}{C_{init}} \frac{6}{v_d d} K_G \left( \frac{Y_{CO_2}}{1 + Y_{CO_2}} - \frac{P^*}{P_{tot}} \right)$$
 (17)

To solve the above set of differential equations for  $Y_{CO_2}$  and  $\alpha$ , gas properties are obtained for humid CO<sub>2</sub> + N<sub>2</sub> mixtures at given CO<sub>2</sub> concentration. The humidity of gas stream was estimated to be at saturated conditions and the details for the same are provided in the Appendix. Liquid properties such as  $D_{CO_2,MEA}$  and  $H_{CO_2,MEA}$  are obtained using the N<sub>2</sub>O analogy wherein the properties are measured for CO<sub>2</sub> and N<sub>2</sub>O in water, and then for N2O in amine. The ratio of property values for CO2 and N2O in water, along with those of N<sub>2</sub>O in amine is used to obtain the properties of CO<sub>2</sub> in amine, as directly measuring the properties of CO<sub>2</sub> in amine is challenging due to its reactivity. The detailed procedure for the same is described in Ko et al. (2001), which provides these relations as functions of temperature. The velocity of the droplet was evaluated assuming Stokes flow with drag and gravity being the main forces acting on the droplet as shown in Eq. (18). The jet velocity was provided as the initial condition for the velocity equation. Gas properties were based on prescribed inlet CO<sub>2</sub> concentration of gas. The velocity was found to reach terminal velocity within 20% of the channel height.

$$\rho_{w}V_{d}g - 6\pi\rho_{g}v_{g}d(v_{d} + U_{G}) = \rho_{w}V_{d}\frac{d(v_{d})}{dt}$$

$$\tag{18}$$

Fig. 2 outlines the procedure for solving the system of equations in the model. Eqs. (14) and (17) can be used to evaluate  $\alpha$  and  $Y_{CO_2}$  along column height. For a given operating condition,  $\alpha_{in}$  and  $Y_{CO_2,in}$  are known. The two equations can be solved as initial value problems (IVP) with solve\_ivp function of the scipy library in Python using a relative tolerance of  $10^{-6}$ . The predictor-corrector method was used to solve the two IVPs. At first, an initial guess of  $Y_{CO_2,out}$  was used along with the prescribed inlet loading. The velocity profile, liquid flow rate, gas flow rate, and temperature was used to obtain the parameter  $K_G(z)$  in Eqs. (14) and (17). The final solution of the IVP evaluated  $Y_{CO_2}(@z = H) = Y_{CO_2,in,pred}$  which is also known for operating systems. The iterated  $Y_{CO_2,in}$  was compared with the given  $Y_{CO_2,in}$  and the residual was minimized to  $10^{-5}$  using the minimize function in scipy library. Once the residual was minimized, the final profiles for  $K_G(z)$ ,  $Y_{CO_2}(z)$ and  $\alpha(z)$  were obtained. These were used to obtain overall volumetric mass transfer performance and capture efficiency of the system as:

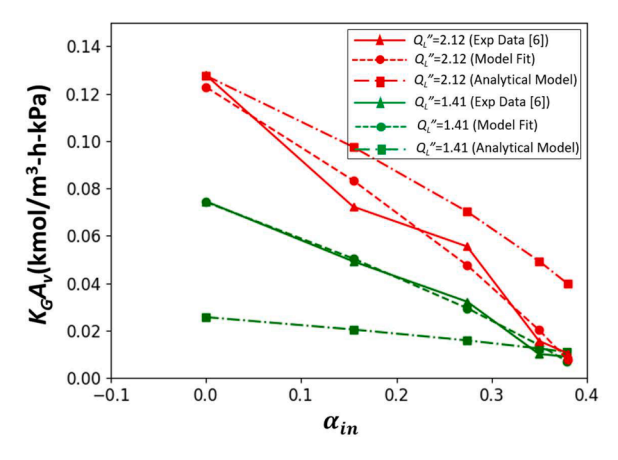
$$K_G A_v = \left(\frac{G_I}{P_{tot} X_{CO_2} - P^*}\right) \left(\frac{dY_{CO_2}}{dz}\right) \tag{19}$$

$$\eta(\%) = \frac{X_{CO_2,in} - X_{CO_2,out}}{X_{CO_2,in}} 100$$
 (20)

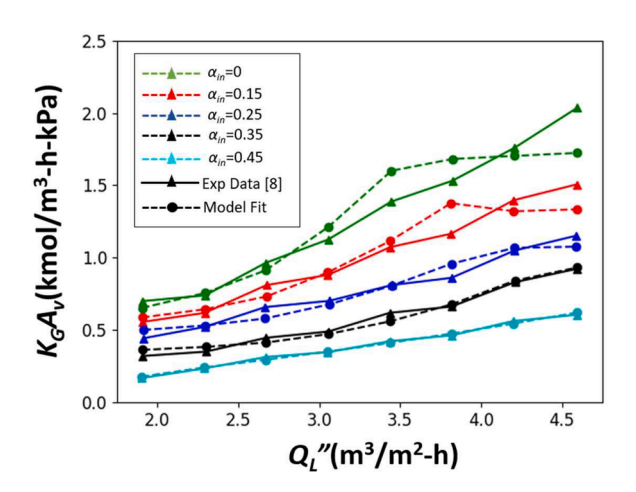
The model can be used to study the influence of many relevant design parameters on the overall performance of the system. It also allows an understanding of the variation of performance parameters such as  $K_G$  and  $A_{\nu}$  along the channel height. Furthermore, it can be used to understand the influence of  $P^*$  on a given system. While the model does account for a lot of the physics and chemistry accompanying carbon capture using sprays, it should be noted that the methodology adapted is based on the following assumptions:

Table 2
Relevant parameters for experiments conducted in (Tamhankar et al., 2015, Kuntz and Aroonwilas, 2009).

Reference	Channel Diameter	Channel Height	Nozzle used	Inlet CO <sub>2</sub> Composition	Temperature	Gas Flow Rate (m <sup>3</sup> /m <sup>2</sup> -h)	Liquid Flow Rate $(m^3/m^2-h)$	Inlet solvent loading	SMD (µm)
(Tamhankar et al., 2015)	0.2 m	3.7 m	BETE MPL 0.30N	12 mol%	30 °C	609.8	1.41, 2.12	0 - 0.38	146- 194
(Kuntz and Aroonwilas, 2009)	0.1 m	0.55 m	BETE P-20, P-28	5-15 kPa	25 °C	382 - 764	1.9 – 10.3	0 – 0.45	88-165



**Fig. 3.** Match between experimental and modeling-based values of  $K_GA_v$  versus  $\alpha_{in}$  for MPL 0.30 N nozzle and two different liquid flow rates in Tamhankar et al. (2015).



**Fig. 4.** Match between experimental and modeling-based values of  $K_G A_v$  versus  $Q_L^r$  for P-28 nozzle and range of inlet loading in Kuntz and Aroonwilas (2009) (dashed lines represent model's fit and the solid lines represent experimental data).

- Droplet-droplet interactions are neglected. Liquid flow is assumed to spread out into equally sized droplets with the diameter equal to the Sauter mean diameter provided by the manufacturer. Due to the lack of manufacturer's data about nozzle specifications, droplet-droplet interactions could not be modeled.
- Spray breakup was considered only to the extent of using the Sauter mean diameter for the working conditions. Initial velocity of each droplet was evaluated from the jet velocity. This assumption overestimates the overall absorption in the region close to the nozzle.
- The Re of droplets for conditions simulated in this work is greater than 1 (lies in the range 2-20). However the Stokes flow approach is used to estimate droplet velocity. While the Stokes flow approach typically requires Re<1, we use it presently as it enables meaningful analysis.

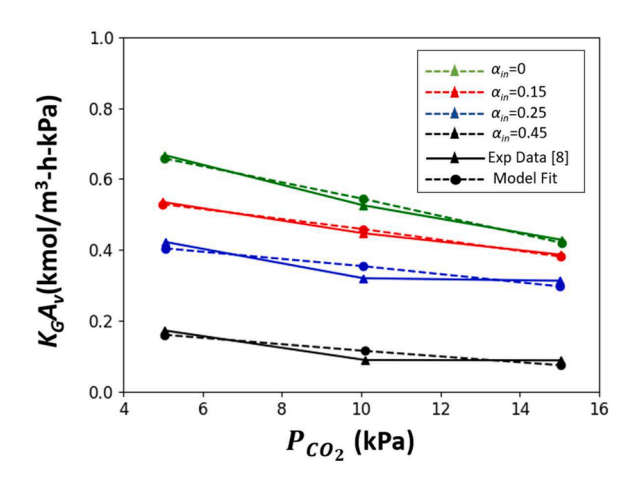


**Fig. 5.** Match between experimental and modeling-based values of  $K_GA_v$  versus  $P_{CO_2}$  (kPa) for P-20 nozzle and range of inlet loading in Kuntz and Aroonwilas (2009)) (dashed lines represent model's fit and the solid lines represent experimental data).

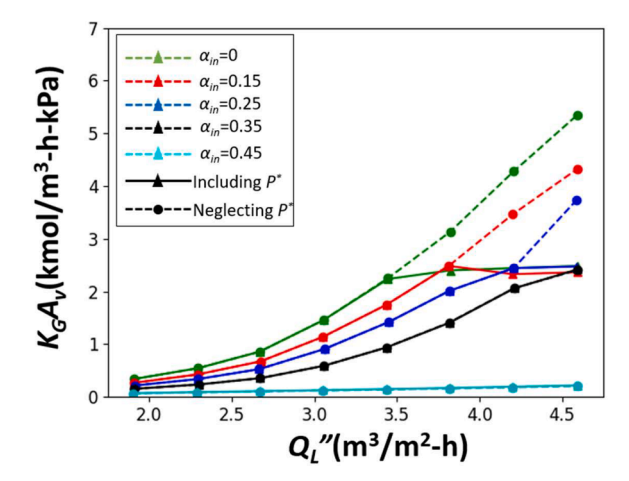


**Fig. 6.** Influence of inclusion/exclusion of  $P^*$  on the outputs of the model (dashed lines represent model predictions neglecting  $P^*$  and the solid lines represent predictions including  $P^*$ ).

- Temperature variation along column height was neglected, and temperature was assumed to be constant and equal to the inlet temperature everywhere. Future studies can examine this assumption in greater detail; if needed temperature variations can be included using the energy equation.
- Evaporation of amine and water was calculated to be negligible. It was found that the gas stream gets saturated with water vapor within 1% distance as soon as it enters the channel. Therefore, gas properties were used for saturated gas. The corresponding change in droplet diameter for the gas to attain saturation was less than 1% and therefore neglected. The evaporation analysis conducted in this study is described in the Appendix.
- A sub-model used in this study Eq. (5) is valid only in the pseudo-first order regime. This requires  $3 < \text{Ha} < < E_{\infty}$ , where Ha and  $E_{\infty}$  can be

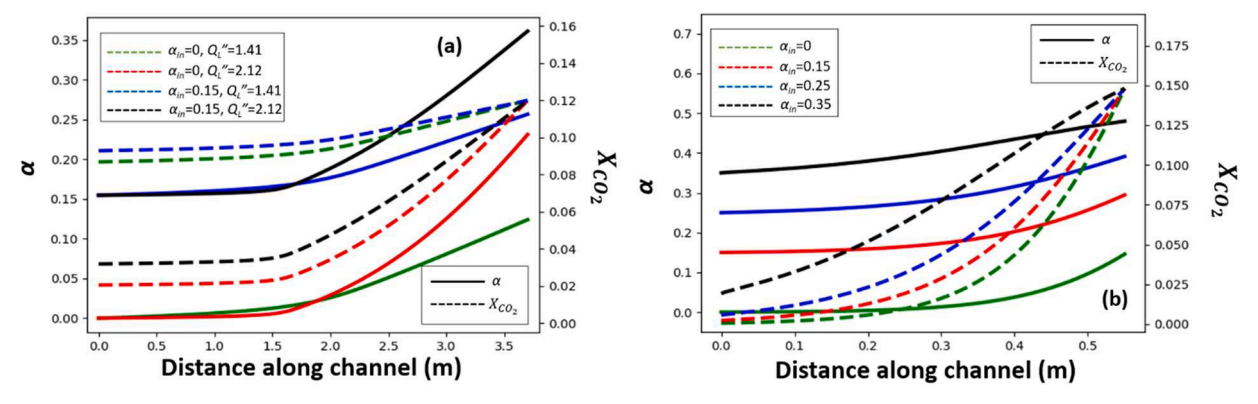


**Fig. 7.** Variation of  $\alpha$  (solid line, left axis) and  $X_{CO_2}$  (dashed line, right axis) along channel height using model's validation for (a) (Tamhankar et al., 2015), and (b) (Kuntz and Aroonwilas, 2009).

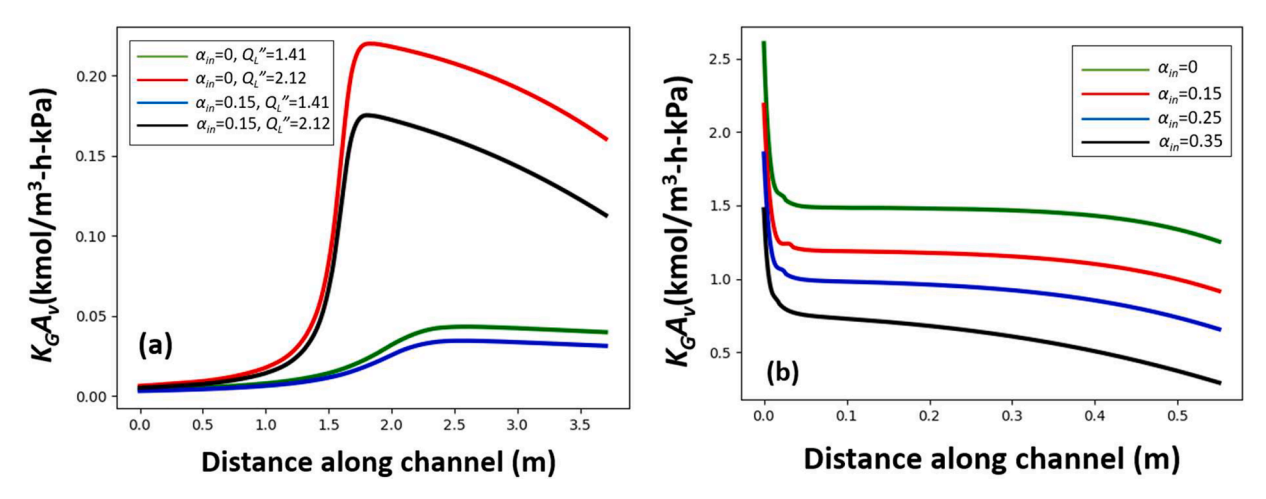


Fig. 8. Variation of  $K_GA_v$  along channel height using model's validation for (a) (Tamhankar et al., 2015), and (b) (Kuntz and Aroonwilas, 2009).

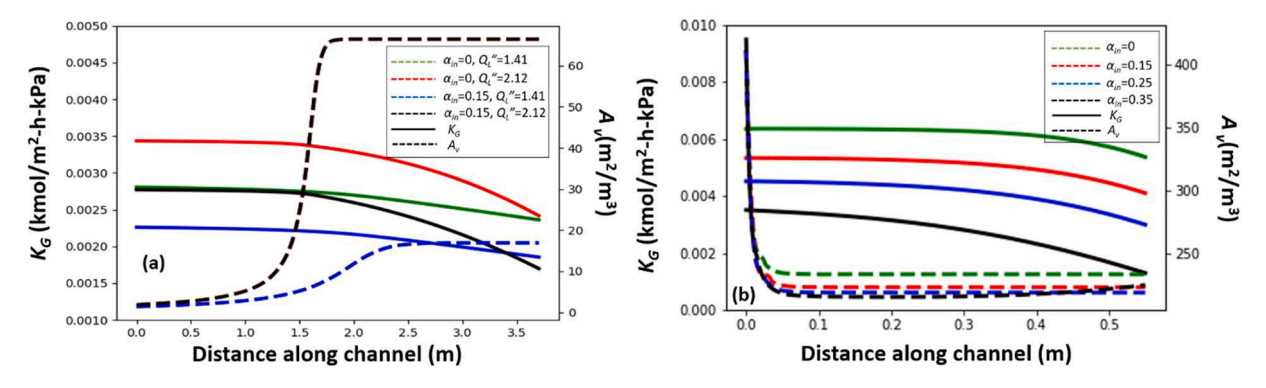


Fig. 9. Variation of  $K_G$  (solid line, left axis) and  $A_\nu$  (dashed line, right axis) along channel height using model's validation for (a) (Tamhankar et al., 2015), and (b) (Kuntz and Aroonwilas, 2008, Kuntz and Aroonwilas, 2009).

obtained from Eqs. (21) and (22) below (Ramezani et al., 2021, Luo et al., 2015). Both these inequalities suggest that the pseudo-first order regime will not hold when loading approaches 0.5. Using this model in those regimes causes oversimplifications such as  $K_G A_{\nu}$  approaching 0 (Figs. 8 and 9). It is noted that this is useful to identify the regimes where overall absorption is relatively lower, even though it is not necessarily 0.

$$Ha = \frac{\sqrt{k_2 C_{init} D_{CO_2} (1 - 2\alpha)}}{k_l}$$
 (21)

$$E_{\infty} = 1 + \frac{D_{MEA}C_{init}(1 - 2\alpha)}{bD_{CO_s}C_{CO_s}^i}$$
(22)

• Only variation in axial direction was considered. The model was lumped in the radial direction since D<<H and both liquid and gas flows are primarily in the axial direction.

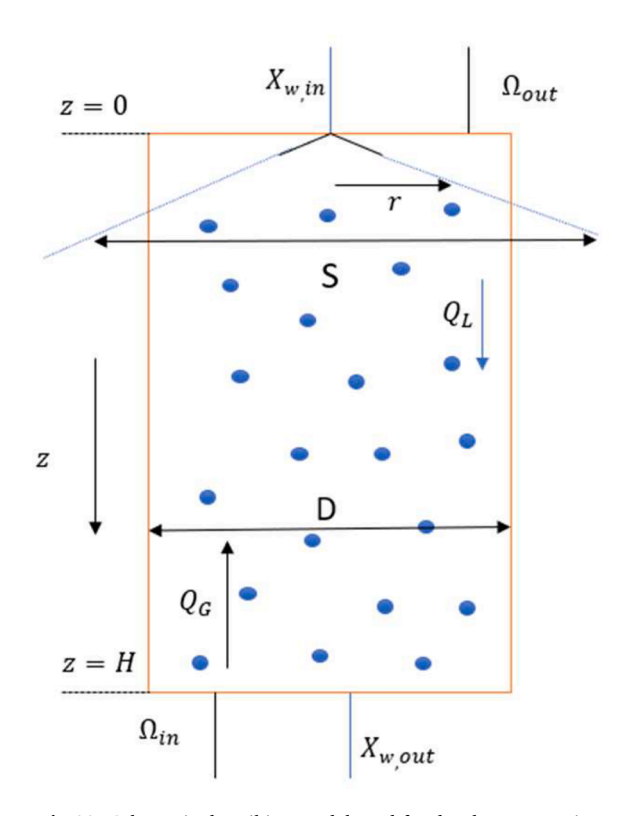


Fig 10. Schematic describing model used for droplet evaporation

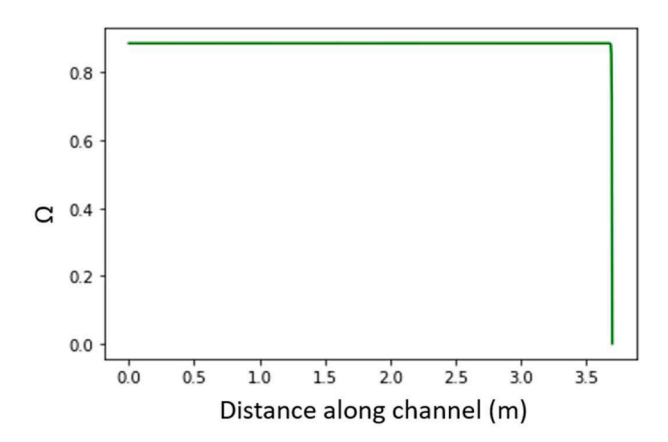


Fig 11. Relative Humidity of gas stream along the channel

#### 3. Results and Discussion

#### 3.1. Validation of the model

The analytical model was validated against the experimental data from (Tamhankar et al., 2015, Kuntz and Aroonwilas, 2009). Both these studies utilize 30 wt% MEA in a spray column at atmospheric pressure with a nozzle on top of the column and gas stream flowing counter-current to liquid flow. Key experimental parameters for the two studies are listed in Table 2 below. Overall performance of system ( $K_GA_V$ ) was studied as a function of liquid flow rates, inlet solvent loading, and inlet partial pressure of  $CO_2$ .

The model was first compared against the experimental results in Tamhankar et al. (2015) and it was observed that trends in  $K_GA_\nu$  with inlet loading are well-predicted as shown in Fig. 3. Model was found to perform reasonably well or slightly overpredict for the higher liquid flow rate but was found to underpredict for lower liquid flow rates. This

can be attributed to the model not including the effect of droplet-droplet interactions. As the liquid flow rate is increased, the droplet density in the channel increases, the SMD of the spray decreases, and the droplet velocity decreases, causing an increase in residence time and a decrease in impact energy. All these effects will cause droplet-droplet interactions to promote more droplet coalescence (Lefebvre and McDonell, 2017, A., 2012). Droplet coalescence will cause a reduction in available surface area for absorption, and therefore an overprediction is observed in the results of the model. The opposite will happen for lower liquid flow rates causing further droplet breakdown and therefore an increase in available contact area, leading to an underprediction by the model.

The analytical model also underpredicts for lower inlet loading conditions. This was because any formation of liquid films on the channel walls was neglected, and its contribution to  $K_GA_V$  would be much more prominent in lower solvent loading conditions. To circumvent these limitations, slope and bias correction fitting factors were added to the analytical model as described in Eq. (23) below. Upon the addition of fitting parameters, the trends were in much more agreement with the experiments.

$$K_G A_v|_{fit} = m * K_G A_v|_{analytical} + c$$
(23)

Next, the variation with liquid flow rate was studied; the match of the model with experiments in Kuntz and Aroonwilas (2009) is depicted in Fig. 4. For these experiments, inlet  $\mathrm{CO}_2$  partial pressure of 15kPa was used along with the P-28 nozzle. A match with 15% error margin with the experimental data was observed, with significant deviations only in regions of high liquid flow rate and low solvent loading due to the same reasons mentioned before. Using the model's fit, the optimal operating conditions can be evaluated for P-28 nozzle, given inlet  $\mathrm{CO}_2$  partial pressure, and design parameters.

Finally, the model was compared with data over a range of inlet  $\rm CO_2$  partial pressures and solvent loading conditions from Kuntz and Aroonwilas (2009). The corresponding experiments were conducted with P-20 nozzle, liquid flow rate of  $1.53~\rm m^3/m^2$ -h, and gas flow rate of  $382\text{-}764~\rm m^3/m^2$ -h. The model predicted the trends extremely well as seen in Fig. 5. This implies that model predictions can be extrapolated to estimate the system's performance at other operating conditions such as those in Direct Air Capture where the  $\rm CO_2$  partial pressures are much lower. This also helps identify the ideal operating conditions for the given system.

## 3.2. Inferences from the model

The influence of considering the equilibrium partial pressure of  $\mathrm{CO}_2$  on the overall mass transfer is shown in Fig. 6. The analytical results were considered with the inclusion and exclusion of  $P^*$  to understand its relative importance for a range of inlet loading and liquid flow rates. It was observed that the influence is prominent only for higher flowrates and at lower  $\mathrm{CO}_2$  loadings, where the overall mass transfer coefficient is high. This is because the driving force  $P_{\mathrm{CO}_2} - P^*$  is small enough only when the overall removal is high causing  $P_{\mathrm{CO}_2}$  to be comparable to  $P^*$ . In the scenario when overall removal is low due to lower overall mass transfer coefficient,  $P_{\mathrm{CO}_2} >> P^*$  and the influence of  $P^*$  is negligible, as observed with low liquid flow rates and at high  $\mathrm{CO}_2$  loadings.

To obtain further insights from the model, two sets of cases were studied in detail. For the first case, the experimental data from Tamhankar et al. (2015) and the model's prediction was considered. This corresponded to an inlet loading of 0, 0.15, and a flux of liquid flow rate equal to 1.41 and 2.12 m³/m²-h which corresponds to an SMD of 193 and 146  $\mu$ m, respectively. The second case studied was the model's validation for experimental data of Kuntz and Aroonwilas (2009) for P-28 nozzle, flux of liquid flow rate of 3.05 m³/m²-h, flux of gas flow rate of 382 m³/m²-h, and a droplet SMD of 113  $\mu$ m. The model was used to obtain variation of mole fraction ( $X_{CO_2}$ ), CO<sub>2</sub> loading ( $\alpha$ ), volumetric overall mas transfer coefficient ( $K_GA_V$ ), total mass transfer coefficient

 $(K_G)$ , and volumetric effective area  $(A_\nu)$ , along channel height. The results for the same are depicted in Figs. 7–9, with subfigures (a) and (b) corresponding to the two cases respectively. From Fig. 7a, it is seen from the flat lines until the middle of the reactor that the majority of  $CO_2$  consumption occurs in the second half of the reactor for all the four conditions shown. This is not true for the other case when the channel height is only 0.55 m compared to 3.7 m. For the shorter reactor, the consumption takes place throughout the channel. This implies that for the given parametric space in operating conditions, the channel in case b could use an addition to its height while the one in case a is already beyond what is needed.

The  $K_GA_v$  for two cases is shown in Fig. 8a and 8b. The first case shows a much lower  $K_GA_v$  than the second case. This is due to a smaller SMD of 113 µm in the first case compared to a higher SMD of 146-193 µm in the second case. Furthermore, the liquid-to-gas flow rate is higher for the second case which also results in a higher  $K_GA_V$ . Fig. 8a shows a very low  $K_GA_v$  in the first half of the reactor followed by a peak around the middle of the channel, while Fig. 8b shows a steady decrease in the  $K_GA_v$  with a peak only at the beginning of the reactor. The overall  $K_GA_v$  and  $K_G$  were used to obtain  $A_v$  along channel height and the results are shown in Fig. 9. It is found that  $K_G$  plateaus in second half of the reactor for the first case with a maximum at the middle of the channel, and  $A_{\nu}$  reduces along the channel height. Fig. 9a shows  $A_{\nu}$  to approach 0 in the top half of the channel. This is because absorption is predominant in the bottom half of the channel where the inlet gas has a higher pressure gradient for absorption. This is also seen in Fig. 7a where both  $\alpha$ and  $X_{CO_2}$  become constant in the top half of the reactor. This results in negligible absorption in the top parts causing a perceived reduction in  $A_{\nu}$ , (while in reality the lack of absorption is due to negligible pressure difference (between gas and liquid streams)) resulting in a low  $K_GA_V$ prediction by the model (as also depicted in Fig. 8a). Since  $A_v$  is evaluated from  $K_GA_{\nu}$  and  $K_G$ , it goes to 0 when  $K_GA_{\nu}$  goes to 0. It is noted that the result of  $K_GA_v$  approaching 0 is partially due to the use of sub-models valid in the pseudo-first regime which does not necessarily hold in the entire domain. Even though  $K_GA_V$  is not exactly 0 in this region, it is still significantly lower than the rest of the reactor suggesting the lack of absorption in this region. For case b,  $K_G$  follows similar trends as  $K_GA_V$ and the effective area was again found to behave similar to case a. Fig. 9 also shows that the effective area changes significantly with increase in liquid flow rate. It is also found to change only slightly with loading, but this can be attributed to the fact that the way it is evaluated is using  $K_GA_V$ and  $K_G$  which vary significantly along channel height and inlet loading. The volumetric effective area was found to be in the range 225-425 m<sup>2</sup>/  $m^3$ , which was found to be close to the range of 100-300  $m^2/m^3$  reported in Kuntz and Aroonwilas (2008).

#### 4. Conclusions

The present study developed a novel analytical model for spray-

based CO<sub>2</sub> capture systems. The utility of the model in predicting performance-related parameters was compared with experimental data from previous studies. The result of including  $P^*$  on the computed performance  $(K_G A_v)$  was also studied and was found to be significant only at high liquid flow rate and low solvent loadings, which correspond to high overall CO<sub>2</sub> capture. The variation of key parameters such as  $K_GA_V$ ,  $K_G$ ,  $A_{\nu}$ ,  $\alpha$ ,  $X_{CO_2}$  along the channel height of the absorber was studied and it was found that in some cases only parts of the absorber are truly utilized for CO2 capture. This provides insights for designing absorbers for specified operating conditions. The model can be used to obtain  $K_GA_V$  for operating conditions over a wider range than those considered in the experimental studies analyzed in this work. This data can then be used to obtain the optimum flow conditions for a given system to maximize CO2 capture rate with respect to energy consumed and/or amount of solvent used. The model can also be used to predict performance of the system with solvent blends if the relevant kinetic and thermophysical properties of the solvent blend are known. Kinetic and thermophysical properties of the solvent blend would be needed to use this model. Properties of interest would include diffusivity in CO2, solubility, viscosity, rate constant of the rate-limiting step in CO2 absorption, etc. Properties are not well-known for solvent blends which would necessitate measurements, but the overall framework of the model can stay the same with only the properties changing. Predictions from this model can also be the basis for techno-economic analysis of sprays-based CO2 absorbers.

## CRediT authorship contribution statement

**Awan Bhati:** Conceptualization, Methodology, Software, Validation, Writing – original draft. **Serhat Bilyaz:** Methodology, Software, Writing – original draft. **Vaibhav Bahadur:** Conceptualization, Writing – review & editing, Supervision, Project administration.

#### **Declaration of Competing Interest**

The authors declare that they have no known competing financial interests or personal relationships that could have appeared to influence the work reported in this paper.

## Data availability

Data will be made available on request.

## Acknowledgements

The authors would like to acknowledge Peter Mathews, Tejaswi Soori, Mark Hamalian, Karey Maynor, Yasmin Bibi, Palash Acharya and Aritra Kar for their support of this project. Prof. Bahadur would also like to acknowledge NSF CBET 1605789 for partial support of this work.

## Appendix: Evaporation of droplet inside the reactor

To understand the effect of evaporation in an amine-water droplet, the system as shown in Fig. 10 is considered where the air stream enters with 0 relative humidity ( $\Omega_{in} = 0$ ), and the liquid stream enters with water mole fraction of 0.88 ( $X_{w,in} = 0.88$ ). The outlet conditions of gas and liquid side are unknown. The rate of evaporation of each of the contained species (MEA and water) would be governed by the Eq. (24) where the subscript i would be either for MEA or for water, m is mass of each droplet,  $h_m$  is the mass transfer coefficient for water evaporation obtained from Sherwood number correlations for a falling droplet,  $\rho_{i,s}$  is the density of species i in gas stream needed for saturation.

$$\frac{dm_i}{dt} = -h_m A_d \rho_{i,s}(X_i - \Omega_i) \tag{24}$$

Upon plugging the respective numbers for MEA and water, it can be safely said that the rate of evaporation of amine is orders of magnitude smaller than that for water. Thus, only the evaporation of water is considered in this work. Furthermore, to solve Eq. (24) for water, both mole fraction and relative humidity can be expressed as functions of m. Since evaporation of amine is much smaller than water, the mass of amine in a liquid droplet can be considered as a constant while evaluating water evaporation, resulting in Eq. (25).

$$m_{MEA} = (1 - Y_w) * m = (1 - Y_{w,i}) * m_i$$
 (25)

Where  $Y_w$  and  $Y_{w,i}$  are the mass fractions of water at distance z and at inlet (z = 0) respectively. The mass fraction along with molecular weights for water and amine can be used to estimate mole fractions upon assuming no  $CO_2$  capture for the evaporation model as a simplification. This assumption is later found to be justified as evaporation is much faster than  $CO_2$  absorption. The relative humidity in gas can be expressed as the ratio of the rate of water vapor flowing out from amine solution ( $m_{wv,out}$ ) to the rate at which it would be needed to be flowing to attain saturation conditions in the gas side ( $m_{wv,sat}$ ), as shown in Eq. (26).

$$\Omega = \frac{m_{wv,out}}{m_{wv,sat}} \tag{26}$$

The net rate of water evaporation from amine can be expressed using the rate of droplet generation ( $\dot{N} = Q_L/V_{d_0}$ , where  $V_{d_0}$  is the volume of droplet at z=0) and the change in mass of individual droplet (m- $m_f$ ) since the only change in mass of droplet is due to water evaporation, it being orders of magnitude faster than amine evaporation. Therefore, the relative humidity at distance z can be expressed as shown in Eq. (27).

$$\Omega = \frac{\dot{Q}_L(m - m_f)}{V_{d_0} \rho_{w,s} \dot{Q}_G} \tag{27}$$

To estimate the maximum possible evaporation, the relative humidity in gas stream would reach the mole fraction of water at inlet conditions. This gives the minimum possible final mass of each individual droplet as shown in Eq. (28).

$$m_{f,\min} = m_i - \frac{X_{w,in}\rho_{w,s}V_{d_0}\dot{Q}_G}{\dot{Q}_L}$$
(28)

Upon plugging in the inputs from the cases studied in this work into the equation, it is found that the change is mass of individual droplet is less than 1% for all the working conditions. This is because the liquid to gas flow rate ratios used for carbon capture are high enough such that the gas gets saturated from negligible change in mass of individual liquid droplets. Next, to identify the distance from gas inlet where it would saturate, the change in relative humidity can be expressed in terms of change in droplet mass as shown in Eq. (29).

$$d\Omega = -\left(\frac{\dot{Q}_L}{\dot{Q}_G V_{d_0} \rho_{w.s}}\right) dm \tag{29}$$

Substituting this into Eq. (24), and using velocity of gas, we get the variation in relative humidity along column height as shown in Eq. (30) below. Upon considering the size of the droplet to be a constant, and solving the below equation as an initial value problem, it is found that the relative humidity reaches saturation in less than 1% of the channel height. This is shown in Fig. 11 for liquid flow rate and gas flow rate of 2.12 and 609.8 m $^3$ /m $^2$ -h respectively used in Tamhankar et al. (2015). This means that for the entire domain, the gas side can be assumed to be saturated. The same conclusion was attained for all other cases studied in this work.

$$\left(\frac{d\Omega}{dz}\right) = \frac{h_m A_d}{U_{gas} V_{d_0}} \frac{\dot{Q}_L}{\dot{Q}_G} \left(X_w - \Omega\right) \tag{30}$$

#### References

- Chen, J.C., Fang, G.C., Tang, J.T., Liu, L.P., 2005. Removal of carbon dioxide by a spray dryer. Chemosphere 59 (1), 99–105. https://doi.org/10.1016/j. chemosphere.2004.09.076.
- Chen, W.H., Tsai, M.H., Hung, C.I., 2013. Numerical prediction of CO2 capture process by a single droplet in alkaline spray. Appl. Energy 109, 125–134. https://doi.org/ 10.1016/j.apenergy.2013.03.082.
- J. Davison, P. Freund, and A. Smith, "Putting carbon back into our soils," IEA Greenh. Gas R&D Program.
- Demontigny, D., Tontiwachwuthikul, P., Chakma, A., 2005. Comparing the absorption performance of packed columns and membrane contactors. Ind. Eng. Chem. Res. 44 (15), 5726–5732. https://doi.org/10.1021/ie040264k.
- Flagiello, D., Parisi, A., Lancia, A., Di Natale, F., 2021. A review on gas-liquid mass transfer coefficients in packed-bed columns. ChemEngineering 5 (3). https://doi. org/10/2390/chempengines/ps/20043
- Garg, S., Murshid, G., Mjalli, F.S., Ali, A., Ahmad, W., 2017. Experimental and correlation study of selected physical properties of aqueous blends of potassium sarcosinate and 2-piperidineethanol as a solvent for CO2 capture. Chem. Eng. Res. Des. 118, 121–130. https://doi.org/10.1016/j.cherd.2016.12.013.
- Javed, K.H., Mahmud, T., Purba, E., 2010. The CO2 capture performance of a high-intensity vortex spray scrubber. Chem. Eng. J. 162 (2), 448–456. https://doi.org/10.1016/j.cej.2010.03.038.
- Ko, J.J., Tsai, T.C., Lin, C.Y., Wang, H.M., Li, M.H., 2001. Diffusivity of nitrous oxide in aqueous alkanolamine solutions. J. Chem. Eng. Data 46 (1), 160–165. https://doi. org/10.1021/ie000138x.
- Kuntz, J., Aroonwilas, A., 2008. Performance of spray column for CO2 capture application. Ind. Eng. Chem. Res. 47 (1), 145–153. https://doi.org/10.1021/ ie0617021.
- Kuntz, J., Aroonwilas, A., 2009. Mass-transfer efficiency of a spray column for CO2 capture by MEA. Energy Procedia 1 (1), 205–209. https://doi.org/10.1016/j. egypro.2009.01.029.

- Lefebvre, A.H., McDonell, V.G., 2017. Atomizers.
- Li, Z., Ji, X., Yang, Z., Lu, X., 2019. Experimental studies of air-blast atomization on the CO2 capture with aqueous alkali solutions. Chinese J. Chem. Eng. 27 (10), 2390–2396. https://doi.org/10.1016/j.cjche.2019.01.021.
- Lim, Y., Choi, M., Han, K., Yi, M., Lee, J., 2013. Performance characteristics of CO2 capture using aqueous ammonia in a single-nozzle spray tower. Ind. Eng. Chem. Res. 52 (43), 15131–15137. https://doi.org/10.1021/ie401981u.
- Luo, X., Hartono, A., Hussain, S., Svendsen, H.F., 2015. Mass transfer and kinetics of carbon dioxide absorption into loaded aqueous monoethanolamine solutions. Chem. Eng. Sci. 123, 57–69. https://doi.org/10.1016/j.ces.2014.10.013.
- Ma, S., Zang, B., Song, H., Chen, G., Yang, J., 2013. Research on mass transfer of CO2 absorption using ammonia solution in spray tower. Int. J. Heat Mass Transf. 67, 696–703. https://doi.org/10.1016/j.ijheatmasstransfer.2013.08.090.
- V. A., 2012. Handbook of Atomization and Spray: Theory and Applications 50 (3).
- Niu, Z., Guo, Y., Lin, W., 2009. Experimental studies on CO2 capture in a spray scrubber using NaOH solution. 2009 International Conference on Energy and Environment Technology, ICEET 2009 3, 52–55. https://doi.org/10.1109/ICEET.2009.479.
- Ramachandran, N., Aboudheir, A., Idem, R., Tontiwachwuthikul, P., 2006. Kinetics of the absorption of CO2 into mixed aqueous loaded solutions of monoethanolamine and methyldiethanolamine. Ind. Eng. Chem. Res. 45 (8), 2608–2616. https://doi. org/10.1021/ie0505716.
- Ramezani, R., Bernhardsen, I.M., Di Felice, R., Knuutila, H.K., 2021. Physical properties and reaction kinetics of CO2 absorption into unloaded and CO2 loaded viscous monoethanolamine (MEA) solution. J. Mol. Liq. 329, 115569 https://doi.org/ 10.1016/j.molliq.2021.115569.
- Stolaroff, J.K., Keith, D.W., Lowry, G.V., 2008. Carbon dioxide capture from atmospheric air using sodium hydroxide spray. Environ. Sci. Technol. 42 (8), 2728–2735. https:// doi.org/10.1021/es702607w.
- Tamhankar, Y., et al., 2015. Spray absorption of CO2 into monoethanolamine: Mass transfer coefficients, dropsize, and planar surface area. Chem. Eng. Res. Des. 104, 376–389. https://doi.org/10.1016/j.cherd.2015.08.012.

- Tamhankar, Y., King, B., Whiteley, R., Resetarits, M., Cai, T., Aichele, C., 2014. Aqueous amine spray absorption and droplet distribution data for CO2 capture applications. Energy Procedia 63, 293–300. https://doi.org/10.1016/j.egypro.2014.11.032.
- Versteeg, G.F., Van Dijck, L.A.J., Van Swaaij, W.P.M., 1996. On the kinetics between CO2 and alkanolamines both in aqueous and non-aqueous solutions. An overview. Chem. Eng. Commun. 144 (May 2012), 133–158. https://doi.org/10.1080/
- Wang, C., Perry, M., Rochelle, G.T., Seibert, A.F., 2012. Packing characterization: Mass transfer properties. Energy Procedia 23, 23–32. https://doi.org/10.1016/j. egypro.2012.06.037.
- Wu, X.M., Qin, Z., Yu, Y.S., Zhang, Z.X., 2018. Experimental and numerical study on CO2 absorption mass transfer enhancement for a diameter-varying spray tower. Appl. Energy 225 (April), 367–379. https://doi.org/10.1016/j.apenergy.2018.04.053.
- Xu, Q., Rochelle, G., 2011. Total pressure and CO2 solubility at high temperature in aqueous amines. Energy Procedia 4, 117–124. https://doi.org/10.1016/j. egypro.2011.01.031.
- Xu, Y., Chen, X., Zhao, Y., Jin, B., 2021. Modeling and analysis of CO2 capture by aqueous ammonia + piperazine blended solution in a spray column. Sep. Purif. Technol. 267 (March), 118655 https://doi.org/10.1016/j.seppur.2021.118655.
- Yates, S.F., Bershitsky, A., Kamire, R.J., 2017. A Closed-Loop CO 2 and Humidity Recovery System for Deep Space Missions," 47th Int. Conf. Environ. Syst. (July 16-20) 1-16
- Yeh, N.K., Rochelle, G.T., 2003. Liquid-phase mass transfer in spray contactors. AIChE J 49 (9), 2363–2373. https://doi.org/10.1002/aic.690490912.
- Zimmermann, S., Schmid, M.O., Klein, B., Scheffknecht, G., 2017. Experimental Studies on Spray Absorption with the Post Combustion CO2 Capture Pilot-Plant CASPAR. Energy Procedia 114 (November 2016), 1325–1333. https://doi.org/10.1016/j. egypro.2017.03.1252.